Nanoscale

PAPER

View Article Online
View Journal | View Issue

Check for updates

Cite this: *Nanoscale*, 2025, **17**, 5161

Investigation of the $Mo_2Ti_2C_3T_x$ MXene in the electrochemical immunosensing of the respiratory syncytial virus (RSV)†

Amina Rhouati,[a] Anupma Thakur,[b] Babak Anasori[b,c] and Mohammed Zourob *[a]

Received 21st October 2024,
Accepted 9th January 2025

DOI: 10.1039/d4nr04333b

rsc.li/nanoscale

MXenes are a growing family of two-dimensional (2D) layered transition metal carbides, nitrides, and/or carbonitrides. Recently, these materials have been used in many sensing and biosensing platforms because of their excellent electrochemical characteristics. In this work, we investigate the applicability of double transition metal (DTM)-based MXenes in the electrochemical immunosensing of the respiratory syncytial virus (RSV). This ubiquitous virus is considered a major pathogen causing acute lower respiratory tract infections in young children and elderly individuals. The immunosensor was constructed by immobilizing the RSV antibody on screen-printed carbon electrodes modified with graphene oxide and the $Mo_2Ti_2C_3T_x$ DTM MXene. The presence of the RSV antigen was detected in a label-free mode using square wave voltammetry. A low limit of detection of 0.015 pg mL^{-1} and a remarkable selectivity against other bacterial and viral pathogens, including coronavirus, were achieved. We also compared this MXene with the standard $Ti_3C_2T_x$ and confirmed that it has a 1.21-fold higher electrochemically active effective surface area. The applicability of the $Mo_2Ti_2C_3T_x$ MXene-based immunosensor in real serum samples was also investigated, yielding excellent recovery percentages ranging from 95.48 to 98.59%.

Published on 03 2 2025. Downloaded on 2026/06/01 19:16:11.

1. Introduction

Since their discovery in 2011, two-dimensional (2D) MXenes have found a wide range of applications in different fields, including supercapacitors, fuel cells, and sensing devices.[1] These 2D materials are characterized by unique optical, mechanical, magnetic, electrical, and chemical properties.[2–4] Chemically, MXenes are a growing family of 2D layered structures composed of transition metal carbides, nitrides, and/or carbonitrides. MXenes are mostly synthesized by wet-chemical selective etching and exfoliation of $M_{n+1}AX_n$, where M refers to the early transition metal, A represents the group 13 or 14 elements and X could be carbon and/or nitrogen.[5] After selective etching of the MAX phase precursor, A layers are removed and the MX multilayers are separated, leading to the single-to-few layer MXene structure $M_{n+1}X_nT_x$, where T_x constitutes the functional groups terminating the MX layers.[6] Since the discovery of the first MXene titanium carbide, $Ti_3C_2T_x$, more than 50 structures have been synthesized.[7]

MXenes can be categorized according to the nature of M and X elements, the thickness of the layers, and the functional groups.[8] Within the MXene structure, the combination of the electronic properties of the $M_{n+1}X_n$ backbone and the surface chemistry of the termination T_x leads to intriguing electrochemical properties including excellent electron transport behavior and a large specific surface area.[9] MXenes are characterized by metal-like conductivity[10] such as ~24 000 S cm^{-1} for the high-quality $Ti_3C_2T_x$ MXene.[11] In addition, it has been reported that the surface dipole moments or electronegativities generated by the functional groups of the termination T_x offer an opportunity for biomolecule and/or nanoparticle immobilization.[12,13] This could be achieved *via* covalent or electrostatic bonds leading to strong anchoring.[10] Many studies have investigated $Ti_3C_2T_x$ MXenes and their hybrids in electrochemical sensing and biosensing devices.[14–16] Excellent analytical performance has been achieved for a wide range of analytes including biomarkers, pathogens, micropollutants, and food contaminants.[7,16] For instance, $Ti_3C_2T_x$ MXenes were investigated in the immunosensing of the carcinoembryonic antigen with a low detection limit of 1×10^{-10}.[17] In another report, the $Ti_3C_2T_x$ MXene was combined with gold nanoparticles to detect miRNA 155 where a detection limit of 0.35×10^{-6} nM was achieved.[18] Despite the fact that MXenes and

[a]*Department of Chemistry, Alfaisal University, Al Zahrawi Street, Al Maather, Al Takhassusi Road, Riyadh 11533, Saudi Arabia. E-mail: mzourob@alfaisal.edu*
[b]*School of Materials Engineering, Purdue University, West Lafayette, IN, 47907, USA*
[c]*School of Mechanical Engineering, Purdue University, West Lafayette, IN, 47907, USA*

† Electronic supplementary information (ESI) available. See DOI: https://doi.org/10.1039/d4nr04333b

Published on 03 2 2025. Downloaded on 2026/06/01 19:16:11.

their hybrids have been investigated in the realm of electrochemical sensors and biosensors, these studies use mostly the $Ti_3C_2T_x$ MXene. $Nb_4C_3T_x$ was also incorporated into the design of the sensing of some analytes, including SARS-CoV-2, dopamine, ascorbic acid, and uric acid.[19–21]

In this work, we aimed to study the applicability of a double-transition-metal (DTM) MXene in electrochemical biosensing. In contrast to mono-transition-metal MXenes, DTMs are composed of two distinct transition metals, differentiated by M′ and M″. M′ and M″ represent the outer and the inner layer metals, respectively, in $M_3C_2T_x$ and $M_4C_3T_x$ MXenes and they can be Ti, V, Nb, Ta, Cr, or Mo. Carbon atoms are sandwiched between the M′ and M″ layers. DTM MXenes have a similar mixture of surface termination groups, such as –F, –O, or –OH as mono-transition metal MXenes.[22,23] Moreover, the diverse structures and variety of transition-metal pairs of DTMs endow them with tunable optical, electric, catalytic and electrochemical properties.[22] Here, the double-transition-metal $Mo_2Ti_2C_3T_x$ MXene was used, and it was synthesized by wet-chemical acid-assisted selective etching of the $Mo_2Ti_2AlC_3$ MAX phase. We combined the $Mo_2Ti_2C_3T_x$ MXene with graphene oxide (GOx) to design an electrochemical immunosensor to detect the respiratory syncytial virus (RSV). GOx was chosen for its numerous functional groups (epoxy, hydroxyl, carbonyl and carboxyl groups), improving the antibody immobilization on the electrode surface.[24]

The developed immunosensor was applied for the detection of the respiratory syncytial virus (RSV). RSV is considered one of the most worrying respiratory RNA viruses with an accentuated mutation process.[25–27] It has been reported as the most frequent viral cause of acute lower respiratory tract infection, in particular in young children and elderly individuals with a worldwide distribution.[28] Some studies demonstrated that RSV infections cannot induce durable protective immunity against further reinfection.[29] For these reasons, this virus is one of the major pathogens that needs to be tackled to prevent the deaths of newborns and children as well as economic losses by 2030.[30] RSV diagnostics is traditionally based on laborious and time-consuming techniques including cell culture, nucleic acid amplification, and immunofluorescence assays. Recently, antigenic tests have been developed to enable rapid and inexpensive *in situ* detection of RSV.[31] Despite their simple principle, these tests are qualitative and lack sensitivity. Therefore, sensitive analytical devices, like electrochemical biosensors, are highly required for the early detection of RSV to develop efficient vaccines and therapies.

2. Materials and methods

2.1. Chemicals and instrumentation

Chemical powders of titanium (−325 mesh, 99.5%), molybdenum (−325 mesh), aluminum (325 mesh, 99.5%), and calcined coke powder (−325 mesh) were purchased from Thermo Scientific and used as received. Deionized (DI) water used in this study was purified using Elix Essential 3 UV, Millipore. Hydrofluoric acid (HF, 48–51% solution in water) and tetramethylammonium hydroxide (TMAOH) solution (25 wt% stock) were purchased from Fisher Scientific and used as received. Anti-RSV monoclonal antibody, RSV inactivated antigen, SARS coronavirus recombinant nucleoprotein, influenza A recombinant nucleoprotein, and inactivated strep A antigen were purchased from Certest Biotechnology, Spain. The antibody and the antigens were diluted in phosphate buffered saline (PBS) solution, pH 7.4. Potassium ferrocyanide $[K_4Fe(CN)_6]$, potassium ferricyanide $[K_3Fe(CN)_6]$, PBS, bovine serum albumin (BSA) and human serum were purchased from Sigma-Aldrich, Germany.

All electrochemical measurements, including cyclic voltammetry (CV), electrochemical impedance spectroscopy (EIS) and square wave voltammetry (SWV), were conducted using a Metrohm (Switzerland) Autolab potentiostat, PGSTAT302N model. The potentiostat was connected to a personnel computer and operated using the Nova 1.11 software. The immunosensor was fabricated on screen-printed carbon electrodes modified with graphene oxide (SPCE/GOx) (Aux: carbon; Ref: Ag) (Metrohm DropSens, Inc. Asturias, Spain).

Field-emission scanning electron microscopy (FESEM) was performed using a JEOL JSM-7800f FESEM with a lower electron detector at an acceleration voltage of 5 kV to study the surface morphology of the electrodes. The samples were gold sputtered to reduce the charging and improve the sharpness of SEM images. Energy dispersive X-ray spectroscopy (EDS) measurements were conducted using an EDAX octane super detector by zooming on individual particles in the SEM imaging to 1000000× zoom with a 30 s exposure time in a point scan. The EDS data were subsequently analyzed using EDAX TEAM software.

2.2. Synthesis and characterization of the $Mo_2Ti_2C_3T_x$ MXene

To synthesize the $Mo_2Ti_2C_3T_x$ MXene, 1 g of the $Mo_2Ti_2AlC_3$ MAX phase was mixed with 10 mL of hydrofluoric acid solution as an etchant in a high-density polyethylene bottle, and stirred at 300 RPM for 96 h at 55 °C. The etched multilayered $Mo_2Ti_2C_3T_x$ MXene flakes were washed with deionized water through repeated centrifugation and decantation in an Eppendorf centrifuge at 3234 RCF (4–5 cycles with ~200 mL of deionized water) until the supernatant reached pH ~ 6. To delaminate, the etched multilayered $Mo_2Ti_2C_3T_x$ MXene sediment was added to 5 mL of TMAOH solution in 15 mL of deionized water per gram of MAX. The mixture of TMAOH and the etched multilayered MXene was then stirred at 300 RPM for 4 h at 55 °C. After delamination, the $Mo_2Ti_2C_3T_x$ MXene solution was washed to neutral pH *via* repeated centrifugation and decantation using a Thermo Scientific centrifuge at 21913 RCF (4 cycles with ~200 mL of deionized water). Thereafter, the final mixture was redispersed in 15 mL of deionized water and vortexed for 15 minutes. The suspension was then centrifuged using the Thermo Scientific centrifuge at 2795 RCF for 30 minutes to ensure that the $Mo_2Ti_2C_3T_x$ MXene solutions were single to few-layered flakes. The final suspension of

 This journal is © The Royal Society of Chemistry 2025

Published on 03 2 2025. Downloaded on 2026/06/01 19:16:11.

$Mo_2Ti_2C_3T_x$ from the supernatant was collected and stored in the freezer at −20 °C until use.

For a comparison study, the $Ti_3C_2T_x$ MXene was also synthesized.[32] Initially, 1 g of optimized Ti_3AlC_2 MAX was first washed using 9 M HCl for 18 h to remove intermetallic impurities and mixed with an etchant solution (6 : 3 : 1 mixture (by volume) of 12 M hydrochloric acid, deionized water, and hydrofluoric acid before stirring at 400 RPM for 24 h at 35 °C. The multilayered etched $Ti_3C_2T_x$ MXene was washed with deionized water *via* repeated centrifugation at 3234 RCF (4–5 cycles with ∼200 mL of deionized water) until the supernatant reached pH ∼ 6. For delamination, the etched multilayered $Ti_3C_2T_x$ MXene sediment was then added to lithium chloride (LiCl) solution, typically 50 mL per gram of the starting etched powder. The mixture of LiCl and the multilayer MXene was then stirred at 400 RPM for 1 h at 65 °C under a constant argon gas flow. The mixture was then washed with deionized water *via* centrifugation at 3234 RCF for 5, 10, 15, and 20 minutes. Then, the final mixture was vortexed for 30 minutes followed by centrifugation at 2380 RCF for 30 minutes to ensure that the $Ti_3C_2T_x$ MXene solutions were single-to-few-layered flakes as shown in Fig. 1b.

The phase purity and composition of $Mo_2Ti_2AlC_3$ MAX and its derived $Mo_2Ti_2C_3T_x$ MXene were analyzed using a Bruker D8 X-ray diffractometer (XRD) with a Cu Kα (λ = 1.5406 Å) emitter and a VANTEC 500 detector. The XRD samples were then mounted on Kapton tapes and scanned from 5° to 80° with a step size of 5° and a time per step of 30 s. The traditional XRD plots were obtained by merging and integrating the XRD^2 data using the DIFFRAC.SUITE EVA software. FESEM was performed using a JEOL JSM-7800f FESEM with a lower electron detector at an acceleration voltage of 15 kV to study the $Mo_2Ti_2AlC_3$ MAX, etched and delaminated $Mo_2Ti_2C_3T_x$ MXene. The solution concentration of the $Mo_2Ti_2C_3T_x$ MXene was maintained at <0.1 mg mL^{-1} and loaded on an anodic disc, followed by vacuum drying for 2 h. The samples were gold sputtered to reduce the charging and improve the sharpness of FESEM images.

2.3. Fabrication of the electrochemical immunosensor and RSV analysis

Scheme 1 depicts the fabrication steps of the $Mo_2Ti_2C_3T_x$ MXene-based immunosensor and its application in the electrochemical determination of the RSV antigen. The electrochemical immunosensor was constructed by adding 10 μL of $Mo_2Ti_2C_3T_x$ MXene solution (3 mg mL^{-1}) prepared in distilled water and sonicated for 10 minutes on the screen-printed carbon electrodes modified with GOx. Then, the surface was allowed to dry at room temperature. Afterwards, the resulting surface of GOx/$Mo_2Ti_2C_3T_x$/SPCE was incubated with 10 μL of the RSV-specific monoclonal antibody (100 μg mL^{-1}) at 4 °C overnight in a water-saturated environment. After that, 1% BSA prepared in PBS, was added to the RSV antibody-functionalized surface to block the non-specific interactions. SPCE electrodes were washed with PBS, pH 7.4, after each modification step. Finally, the immunosensors were stored at 4 °C for further use. Cyclic voltammetry (CV) at a scan rate of 100 mV s^{-1} within a potential range of −0.6 to 0.6 V was used for the characterization of the immunosensor fabrication steps in 5 mM ferro/ferricyanide redox solution prepared in PBS buffer at a pH of 7.4. EIS characterization was also carried out in the same electrolyte, over the frequency range from 10^5 to 1 Hz, a potential of +0.4 V and an amplitude of 10 mV.

The electroactive properties of $Mo_2Ti_2C_3T_x$ were studied and compared to those of the $Ti_3C_2T_x$ MXene. For that, two electrodes were prepared; the first one was modified with $Mo_2Ti_2C_3T_x$ and the second one was modified with the $Ti_3C_2T_x$ MXene. Then, CV was performed at different scan rates ranging from 10 to 100 mV s^{-1}.

For detection experiments, 10 μL of RSV antigen solution was dropped on the SPCE modified with GOx/$Mo_2Ti_2C_3T_x$/RSV-antibody and incubated for 20 minutes at room temperature. Increasing amounts of the RSV antigen ranging from 0 to 10 000 pg mL^{-1} prepared in PBS were tested. After rinsing the surface with PBS, a 5 mM ferro/ferrocyanide redox probe was placed on the immunosensor for electrochemical measurements. Square wave (SWV) measurements were performed in the range of −0.2 to 0.3 V, at an interval time of 0.04 s, a frequency of 25 Hz, a scan rate of 125 mV s^{-1}, an amplitude of 20 mV, and a step potential of −5 mV.

2.4. Cross-reactivity and real sample applicability

To evaluate the specificity of the proposed immunosensor, the RSV-antibody functionalized SPCEs were incubated with 10 μL of the targeted viral antigen and some potential interfering viruses (Flu A, coronavirus, and Strep A), separately, by using the same procedure described above. Then, the immunosensor responses to the different antigens were electrochemically recorded by SWV and compared by determining the change in the peak current after the binding. In parallel, the matrix effects on the immunosensor analytical performance were also studied. The sensor was tested with real serum samples spiked with different concentrations of the RSV antigen. For that, the GOx/$Mo_2Ti_2C_3T_x$/SPCE functionalized with the RSV antibody was incubated with different real serum samples spiked with increasing concentrations of the RSV antigen (0.01, 1, and 25 pg mL^{-1}). Before spiking, the human serum was diluted in PBS (1 : 50). Using the same experimental conditions described above, the electrochemical response was determined for each concentration and used to calculate the recovery percentages.

3. Results and discussion

3.1. Electroactive properties of $Mo_2Ti_2C_3T_x$ and $Ti_3C_2T_x$ MXene materials

In this study, we focused on the synthesis and use of a DTM MXene, $Mo_2Ti_2C_3T_x$. As we mentioned in the Introduction section, many biosensors have been developed by using the $Ti_3C_2T_x$ MXene. Therefore, we prepared an electrode modified with the standard $Ti_3C_2T_x$ to compare its electrochemical properties with those of the $Mo_2Ti_2C_3T_x$-modified surface. Each

Published on 03 2 2025. Downloaded on 2026/06/01 19:16:11.

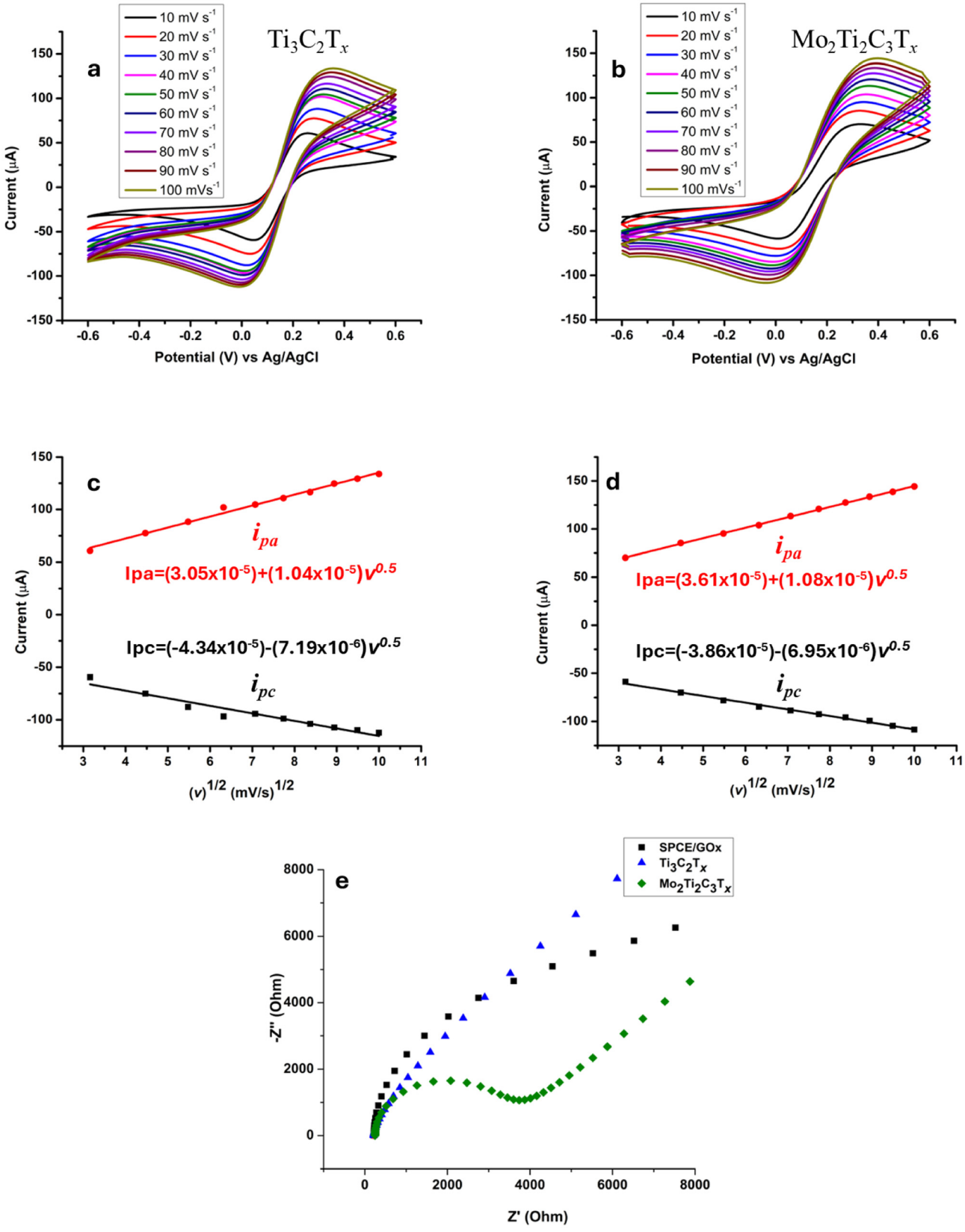

Fig. 1 Cyclic voltammograms of the GOx/SPCE modified with $Ti_3C_2T_x$ (a) and $Mo_2Ti_2C_3T_x$ MXenes (b) performed in 5 mM ferro/ferricyanide redox solution prepared in PBS buffer at a pH of 7.4 (scan rates 10, 20, 30, 40, 50, 60, 70, 80, 90 and 100 mV s^{-1}) and a potential window of −0.6 to 0.6V. Plots of anodic and cathodic peak currents *vs.* the square root of scan rates for $Ti_3C_2T_x$ (c) and $Mo_2Ti_2C_3T_x$ (d). Impedance spectra were recorded for $Ti_3C_2T_x$- and $Mo_2Ti_2C_3T_x$-modified electrodes.

This journal is © The Royal Society of Chemistry 2025

Published on 03 2 2025. Downloaded on 2026/06/01 19:16:11.

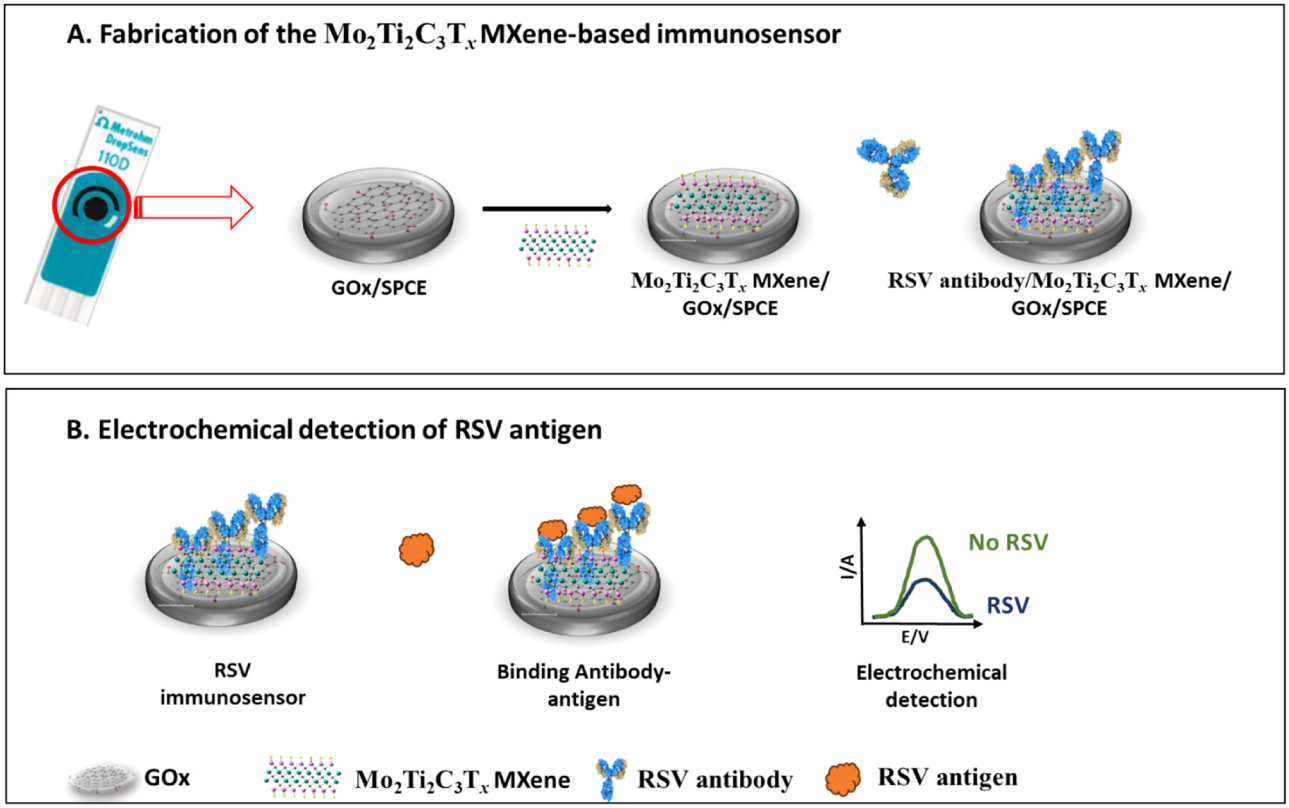

Scheme 1 Schematic illustration of (A) the fabrication steps of the $Mo_2Ti_2C_3T_x$ MXene-based immunosensor and (B) its application in the electrochemical detection of the RSV antigen.

electrode was subjected to cyclic voltammetric analysis by using different scan rates and the recorded voltammograms are shown in Fig. 1a and b, respectively. It is observed that as the scan rate increases, the anodic oxidation peak increases and the cathodic reduction peak decreases. By extracting the oxidation and reduction peak currents, we plotted i_{pa} and i_{pc} fit as a function of the square root of the scan rate ($v^{1/2}$) for the two electrodes. As shown in Fig. 1c and d, a good linearity was obtained for $Mo_2Ti_2C_3T_x$- and $Ti_3C_2T_x$-modified electrodes with an R^2 value of 0.99 for anodic and cathodic curves. The linear equations were determined: $I_{pa} = (3.61 \times 10^{-5}) + (1.08 \times 10^{-5})\, v^{0.5}$ and $I_{pc} = (-3.86 \times 10^{-5}) - (6.95 \times 10^{-6})\, v^{0.5}$ for the $Mo_2Ti_2C_3T_x$-modified SPCE. In parallel, the equations corresponding to $Ti_3C_2T_x$ were as follows: $I_{pa} = (3.05 \times 10^{-5}) + (1.04 \times 10^{-5})\, v^{0.5}$ and $I_{pc} = (-4.34 \times 10^{-5}) - (7.19 \times 10^{-6})\, v^{0.5}$. Based on these outcomes, we suggest a diffusion-controlled process for the modified electrodes.[33]

Given that the quality of the sensing surface depends on the diffusion speed of electrons on the electrode, we used the Randles–Sevcik equation to determine this important parameter by calculating the electroactive surface area.[34]

$$i_{pa} = 2.69 \times 10^5 \times n^{3/2} \times A \times C^{\circ} \times D^{1/2} \times v^{1/2}$$

Based on the equation, i_{pa} is the peak current, n is the number of electrons, A is the active surface area, C° is the concentration of the analyte, D is the diffusion coefficient of the oxidized analyte and v is the scan rate. The electroactive surface area (A) of the two prepared electrodes was estimated according to the equation. In this study, the concentration of [Fe $(CN)_6^{3-}$] solution $C^{\circ} = 5.0 \times 10^{-6}$ mol cm^{-3} was used with the number of electrons $n = 1$. The diffusion coefficient value $D = 3.14 \times 10^{-6}$ was extracted from the plotted curves in Fig. 1c and 2d. The effective surface area was determined as 24 mm^2 and 29 mm^2 for the $Ti_3C_2T_x$- and $Mo_2Ti_2C_3T_x$-modified electrodes, respectively. These findings confirm that the $Mo_2Ti_2C_3T_x$ MXene allows faster electron transfer through the interface sensing surface solution than the $Ti_3C_2T_x$ MXene.

EIS was further implemented for the electrochemical study of the $Ti_3C_2T_x$- and $Mo_2Ti_2C_3T_x$-modified electrodes. The impedance spectra shown in Fig. 2e show the enhanced electron transfer on the $Mo_2Ti_2C_3T_x$-modified surface as compared to $Ti_3C_2T_x$. The Nyquist plots were fitted using a modified Randles equivalent circuit shown in Fig. S2.† We note that the resistance R_{et} increases after the addition of the two MXene materials on the GOx/SPCE surface. The R_{et} of the bare electrode was fitted to be 22.45 kΩ; it decreased to 18.72 kΩ after the addition of $Ti_3C_2T_x$. In parallel, we note a noticeable decrease in the charge resistance transfer R_{ct} (1.87 kΩ) after the surface modification with $Mo_2Ti_2C_3T_x$. These results confirm that the $Mo_2Ti_2C_3T_x$ MXene constitutes an excellent sensing surface and immobilization support for our biorecep-

Published on 03 2 2025. Downloaded on 2026/06/01 19:16:11.

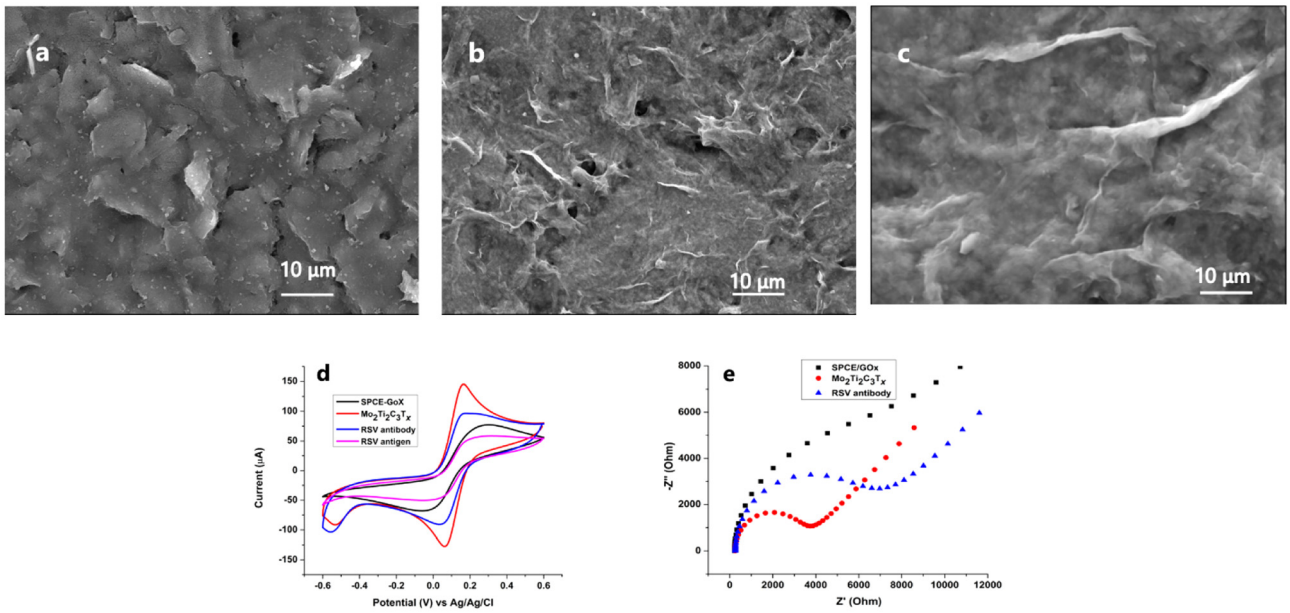

Fig. 2 SEM images of screen-printed electrodes: (a) bare GOx/SPCE, (b) GOx/$Mo_2Ti_2C_3T_x$/SPCE (×1000) and (c) GOx/$Mo_2Ti_2C_3T_x$/SPCE (×2000). The accelerating voltage was 5 kV. (d) Electrochemical characterization corresponding to each step of GOx/$Mo_2Ti_2C_3T_x$/SPCE immunosensor fabrication: the GOx modified-SPCE (black line), the GOx/$Mo_2Ti_2C_3T_x$/SPCE (red line), the GOx/$Mo_2Ti_2C_3T_x$/SPCE immunosensor (blue line) and the GOx/$Mo_2Ti_2C_3T_x$/SPCE immunosensor after binding with the RSV antigen at a concentration of 25 pg mL^{-1} (pink line) using cyclic voltammetry (CV) by scanning the potential between −0.6 V and 0.6 V at a scan rate of 100 mV s^{-1}. (e) EIS characterization corresponding to the GOx modified SPCE (black line), the GOx/$Mo_2Ti_2C_3T_x$/SPCE (red line) and the GOx/$Mo_2Ti_2C_3T_x$/SPCE immunosensor (blue line). EIS spectra were recorded in the same electrolyte, over the frequency range from 10^5 to 1 Hz, a potential of +0.4 V and an amplitude of 10 mV. EIS spectra were fitted using the circuit shown in Fig. S2.†

tor. The EIS analysis results are in good agreement with the study of the electroactive surface area.

3.2. SEM and EDS analyses

The electrode surface was studied before and after the addition of the $Mo_2Ti_2C_3T_x$ MXene by using SEM. Fig. 2a shows the SEM image of the GOx-modified carbon electrode. Single-layer structured GOx with smooth surfaces with folds and wrinkles is visible.[35] After the addition of $Mo_2Ti_2C_3T_x$ on the graphene oxide-modified electrode, we noted the formation of a few layered MXene. SEM images displayed in Fig. 2b and c confirm the layered sheet-like structure of the MXene.

Furthermore, elemental mapping was carried out on SPCE/GOx before and after the addition of $Mo_2Ti_2C_3T_x$ nanosheets by EDS (ESI†). The obtained images show the spatial distribution of Mo, Ti and C. The presence of these elements confirms the successful modification of our SPCE/GOx surface with the $Mo_2Ti_2C_3T_x$ MXene. In parallel, EDS analysis validates the presence of surface termination (O, OH and F). These findings are in good agreement with the electrochemical characterization results, indicating the effect of these chemical groups.

3.3. Electrochemical characterization of the $Mo_2Ti_2C_3T_x$ MXene-based immunosensor

Cyclic voltammetry was used to study the electrochemical behavior of the GOx/$Mo_2Ti_2C_3T_x$ immunosensor. The interfacial charge transfer between the surface and the supporting redox probe of ferro/ferricyanide was evaluated after each step of surface modification. Fig. 1d shows the obtained voltammograms, where the black line corresponding to the carbon electrode surface modified with GOx shows a characteristic reversible redox peak with a peak-to-peak separation (ΔE_p) of 0.38 V. After the addition of the $Mo_2Ti_2C_3T_x$ MXene, we noted an increase in the peak current accompanied by a decrease of the peak-to-peak separation to 0.3 V (red line). The non-electrical conductivity of graphene oxide was compensated by MXene properties. The enhanced charge transfer is certainly due to the synergistic effect of the double transition metals, Mo and Ti, resulting in a large active surface area and electrical conductivity. The electrochemical characteristics of the $Mo_2Ti_2C_3T_x$ MXene could promote electron transfer, inhibit electrolyte decomposition, and maintain electrode structural integrity.[36] The voltammogram recorded after the anchoring of the RSV antibody on the GOx/$Mo_2Ti_2C_3T_x$ MXene-modified SPCEs shows a significant decrease in the peak current with a peak-to-peak separation of 0.72 V due to the proteic nature of antibodies (blue line). This result confirms the successful immobilization of our bioreceptor on the nano-assembly GOx/$Mo_2Ti_2C_3T_x$ MXene. This returns to the abundant functional groups in the graphene oxide structure (epoxy, hydroxyl, carbonyl and carboxyl groups) that enable the covalent interaction of amine groups of the antibody,[24,37] in addition to the functional termination groups of the $Mo_2Ti_2C_3T_x$ MXene (–OH, –O, and –F). Finally, the drop in the peak current and the

 This journal is © The Royal Society of Chemistry 2025

Published on 03 2 2025. Downloaded on 2026/06/01 19:16:11.

increased ΔE_p (0.8 V) observed in the pink line indicates the formation of the complex antibody–RSV antigen and confirms the good orientation of the antibodies immobilized on the GOx/$Mo_2Ti_2C_3T_x$-modified surface.

Voltammetric analysis was supported with electrochemical impedance characterization shown in Fig. 2e. The recorded spectra are in good agreement with the cyclic voltammograms, where we note an increase in the surface resistance and a decrease in the electron transfer after the addition of the RSV antibody (blue line).

3.4. Dose-to-dose response of the RSV immunosensor

Before the application of the $Mo_2Ti_2C_3T_x$ MXene-based immunosensor for RSV determination, the optimization of two key parameters was conducted. First, the amount of the bioreceptor (RSV monoclonal antibody), which strongly affects the sensor sensitivity, was optimized. For that, different concentrations of the RSV antibody, ranging from 50 μg mL^{-1} to 200 μg mL^{-1}, were incubated with the GOx/$Mo_2Ti_2C_3T_x$ MXene-modified SPCEs overnight at 4 °C. The resulting immunosensors were then used for RSV detection, where we observed that low signals were recorded by using small amounts of antibody and a concentration of 100 μg mL^{-1} allowed better detection of RSV with a high signal/noise ratio (data not shown). Therefore, the antibody concentration of 100 μg mL^{-1} was selected to conduct the next experiments. The binding time between the antibody and its antigen is also of critical importance and needs to be optimized. To address this, we tested five incubation durations (5, 10, 15, 20, and 25 minutes) for the interaction between the immunosensor

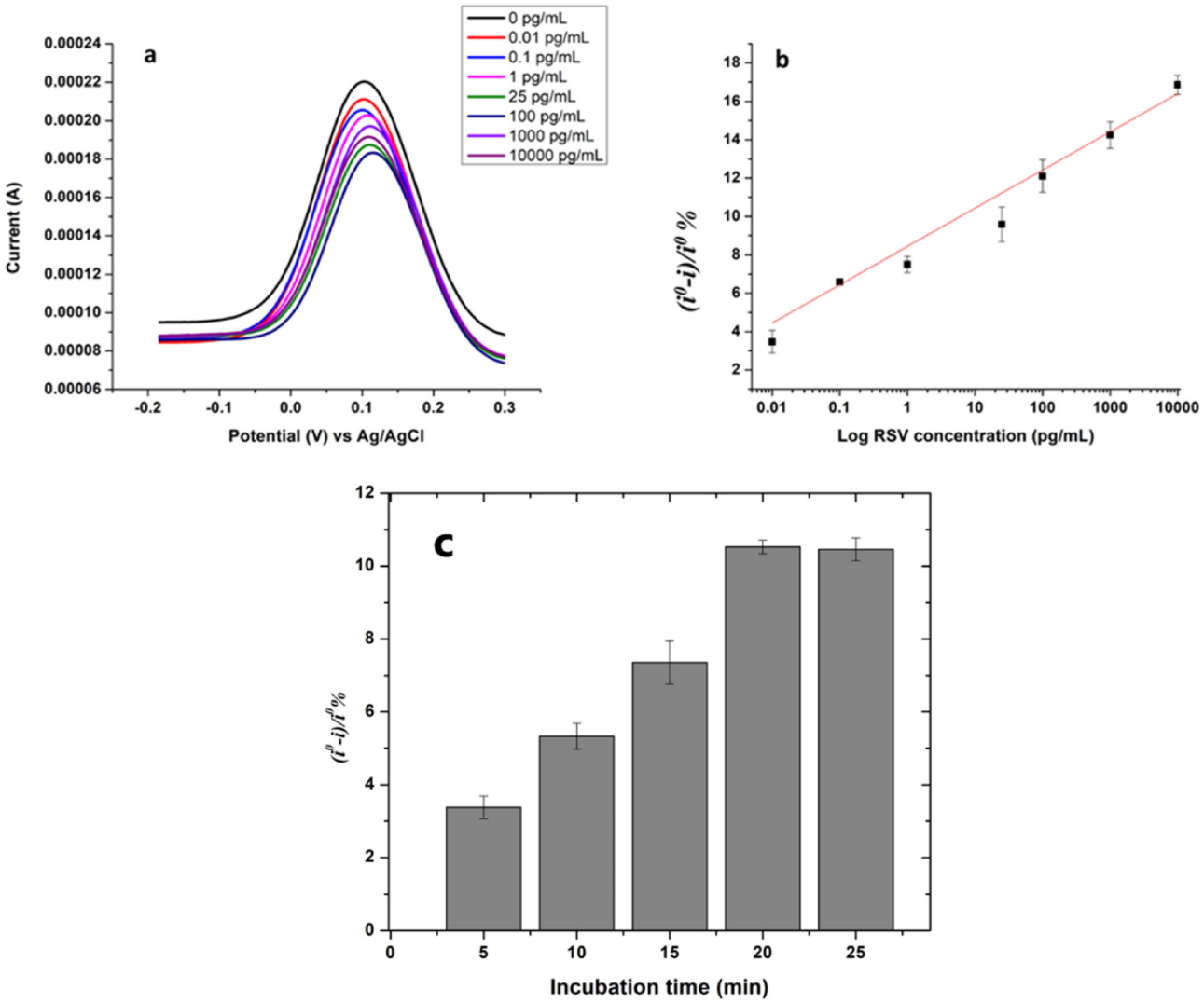

Fig. 3 (a) Square wave voltammograms recorded for the GOx/$Mo_2Ti_2C_3T_x$/SPCE immunosensor towards increasing concentrations of the RSV antigen (0, 0.01, 0.1, 1, 25, 100, 1000 and 10 000 pg mL^{-1}) prepared in PBS. (c) Effect of the binding time on the response of the RSV immunosensor. The measurements were carried out in a 5 mM ferri/ferrocyanide solution in PBS buffer at a pH of 7.4. The measurements were recorded in the ferro/ferricyanide electrolyte in the range of −0.2 to 0.3 V, at an interval time of 0.04 s, a frequency of 25 Hz, a scan rate of 125 mV s^{-1}, an amplitude of 20 mV, and a step potential of −5 mV. (b) Plot of the sensor's response *versus* the logarithm of RSV antigen concentrations.

Published on 03 2 2025. Downloaded on 2026/06/01 19:16:11.

and the RSV antibody. Fig. 3c shows the effect of incubation time on the immunosensor response. The response of the sensor was determined as $(i^\circ - i)/i^\circ\%$, where i° is the electrochemical signal obtained before RSV addition on the immunosensor and i corresponds to the peak current recorded after each incubation time. We noted that the immunosensor exhibited a better response by increasing the incubation time from 5 to 20 minutes, after which, we noted a slight decrease in the response of the biosensor. Consequently, 20 minutes was chosen as the optimum incubation time for the complex antibody–RSV antigen.

Under the optimized experimental conditions, the analytical performance of the proposed $Mo_2Ti_2C_3T_x$ MXene-based immunosensor was studied. For that, the functionalized surface was incubated with different concentrations of the RSV antigen varying from 0.01 pg mL^{-1} to 10 μg mL^{-1} for 20 minutes, separately. After washing with PBS, SWV measurements were conducted in the presence of the redox probe ferri/ferrocyanide by scanning the potential in the range of −0.2 to 0.3 V, at an interval time of 0.04 s, a frequency of 25 Hz, a scan rate of 125 mV s^{-1}, an amplitude of 20 mV and a step potential of −5 mV. In this work, the principle of detection is simple based on monitoring the electron transfer rate variation on the $GOx/Mo_2Ti_2C_3T_x$ MXene-modified SPCEs after the addition of the targeted antigen RSV. Fig. 3a shows the square wave voltammograms recorded before and after the addition of different concentrations of the RSV antigen. As can be seen from Fig. 2a, the peak currents were decreased by increasing the antigen concentration. This decrease confirms the formation of the complex antibody–RSV which hampers electron transfer to the electrode surface.

The obtained peak currents were then used to determine the response of the sensor $(i^\circ - i)/i^\circ\%$, where i° is the electrochemical signal obtained before RSV addition on the immunosensor and i corresponds to the peak current recorded after incubation of each RSV concentration. Afterwards, the calibration curve in Fig. 3b was obtained by plotting the response $(i^\circ - i)/i^\circ$ % *versus* the logarithm of RSV concentration. A good linear relationship was obtained within the range of 0.01 pg mL^{-1}–10 μg mL^{-1} with the regression equation $(i^\circ - i)/i^\circ\% = 8.43 + 1.99 \log[\text{RSV}]$ (pg mL^{-1}) and a coefficient of determination (R^2) of 0.9737. A low limit of detection of 0.015 pg mL^{-1} was also achieved for the proposed RSV immunosensor; it was also calculated as $3\sigma/b$, where σ is the standard deviation of the blank and b is the slope. The excellent analytical performances, mainly the wide linear range and the low limit of detection, could be attributed to the characteristics of the double transition metal $Mo_2Ti_2C_3T_x$ MXene. First, the large surface area and the terminal groups –O and –OH enabled the binding of a large number of capture RSV antibodies. On the other hand, the excellent electronic behavior of this material contributes to enhancing the charge transport and thus amplifying the electrochemical signal.

3.5. Cross-reactivity studies

Aiming to demonstrate the ability of the developed immunosensor to distinguish between different pathogens, Flu A, coronavirus, Strep A, and RSV antigens were separately incubated on the $GOx/Mo_2Ti_2C_3T_x$ MXene/RSV antibody/SPCEs. These pathogens were selected because they are responsible for respiratory infectious diseases. After incubating the antigens with the immunosensing platform, square wave voltammograms were recorded, as demonstrated above. Then, the sensor response $(i^\circ - i)/i^\circ\%$ was determined for each of the non-specific antigens and compared to that obtained for the RSV antigen. As shown in Fig. 4, the sensor response was non-significant for the different interfering antigens even at a concentration of 9 μg mL^{-1}. However, the presence of the RSV antigen at the same concentration on the electrode surface resulted in a drop in the electrochemical signal and thus a major response $(i^\circ - i)/i^\circ\%$. These findings confirm that our immunosensor presents good selectivity towards other respiratory bacteria and viruses. Our strategy would help healthcare practicians in the rapid identification of the specific pathogen and the selection of an appropriate treatment.

3.6. Matrix effect and applicability of the immunosensor in human serum samples

To validate the proposed method and demonstrate its feasibility in complex biological fluids, the $Mo_2Ti_2C_3T_x$ MXene-based immunosensor was tested with real human serum samples. The serum was first diluted 50 times in PBS and spiked with different concentrations of the RSV antigen within the linear range of the immunosensor: 0.01, 1, and 25 pg mL^{-1}. Then, the prepared samples were incubated with the $GOx/Mo_2Ti_2C_3T_x$ MXene-modified SPCEs functionalized with the RSV antibody. Square wave measurements were conducted to analyze the sensor response in the absence and in the presence of different concentrations of RSV-spiked serum samples. Based on the calculated $(i^\circ - i)/i^\circ\%$, a recovery study was carried out to compare the added concentrations and the

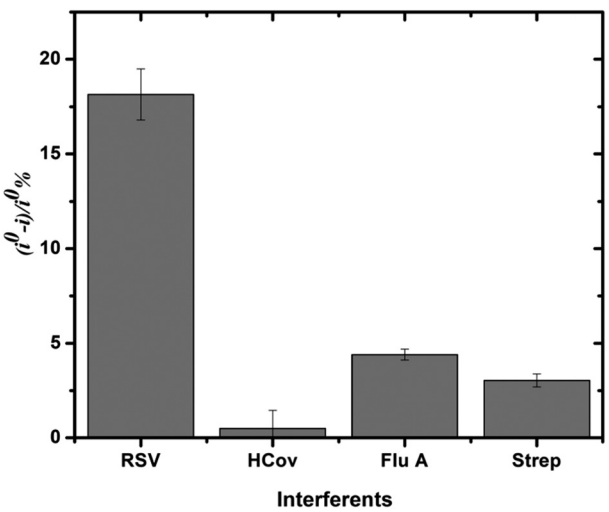

Fig. 4 Specificity of the developed $GOx/Mo_2Ti_2C_3T_x$/SPCE immunosensor against RSV and other antigens coronavirus, Flu A and Strep A at a fixed concentration of 9 μg mL^{-1}.

 This journal is © The Royal Society of Chemistry 2025

Published on 03 2 2025. Downloaded on 2026/06/01 19:16:11.

Table 1 RSV quantification in spiked human serum samples by using the GOx/$Mo_2Ti_2C_3T_x$ MXene/SPCE immunosensor

Added concentration (pg mL^{-1})	Found concentration (pg mL^{-1})	Recovery percentage (%)	Relative standard deviation (%)
0.01	0.0098	98.59	1.33
1	0.98	98	5.29
25	23.86	95.48	1.99

found amounts of the RSV antigen. The recovery percentages obtained for each concentration as well as the relative standard deviation corresponding to the triplicate trials are listed in Table 1. The recovery rates ranging between 95 and 98% with reasonable RSDs confirm that the proposed immunosensor could be applied in clinical analysis without the matrix effect.

4. Conclusions

In summary, a new label-free electrochemical immunosensor was successfully constructed for the detection of the respiratory virus RSV. The double transition metal MXene $Mo_2Ti_2C_3T_x$ offers many binding sites and surface areas for antibody immobilization. In addition, this material exhibits excellent conductivity, thus improving the immunosensor sensitivity. $Mo_2Ti_2C_3T_x$ showed better performance than $Ti_3C_2T_x$, possibly due to more binding and active sites in the surface of $Mo_2Ti_2C_3T_x$. Surface functionalization with the MXene and RSV antibody was characterized by cyclic voltammetry, EIS and scanning electron microscopy. The electrochemical detection of a wide range of RSV antigen concentrations was carried out by square wave voltammetry, leading to a low detection limit of 0.015 pg mL^{-1} and a linear range (0.01 pg mL^{-1} to 10 μg mL^{-1}). The selectivity of the developed immunosensor was also demonstrated against three antigens coronavirus, Flu A and Strep A, known for their respiratory pathogenicity. Moreover, the recovery study in real serum samples confirms the applicability of the $Mo_2Ti_2C_3T_x$ MXene in complex matrices without interfering effects. This immunosensor represents an excellent biomolecular tool for simple, low cost and fast diagnostics of the respiratory syncytial virus. It combines the high affinity of antibodies, the high sensitivity and easy handling of electrochemical devices and the outstanding properties of MXene materials.

Data availability

The data that support the findings of this study are available from the corresponding author upon reasonable request.

Conflicts of interest

There are no conflicts to declare.

References

1 S. Alwarappan, N. Nesakumar, D. Sun, T. Y. Hu and C.-Z. Li, 2D metal carbides and nitrides (MXenes) for sensors and biosensors, *Biosens. Bioelectron.*, 2022, **205**, 113943.
2 B. C. Wyatt, A. Rosenkranz and B. Anasori, 2D MXenes: tunable mechanical and tribological properties, *Adv. Mater.*, 2021, **33**(17), 2007973.
3 K. Hantanasirisakul and Y. Gogotsi, Electronic and optical properties of 2D transition metal carbides and nitrides (MXenes), *MXenes*, 2018, **30**(52), 1804779.
4 A. Champagne and J.-C. J. Charlier, Physical properties of 2D MXenes: from a theoretical perspective, *J. Phys.: Mater.*, 2020, **3**(3), 032006.
5 A. S. Ingason, M. Dahlqvist and J. Rosén, Magnetic MAX phases from theory and experiments; a review, *J. Phys.: Condens. Matter*, 2016, **28**(43), 433003.
6 M. Naguib, V. N. Mochalin, M. W. Barsoum and Y. Gogotsi, 25th anniversary article: MXenes: a new family of two-dimensional materials, *Adv. Mater.*, 2014, **26**(7), 992–1005.
7 L. Lorencova, P. Kasak, N. Kosutova, M. Jerigova, E. Noskovicova, A. Vikartovska, M. Barath, P. Farkas and J. Tkac, MXene-based electrochemical devices applied for healthcare applications, *Microchim. Acta*, 2024, **191**(2), 88.
8 P. O. Persson and J. Rosen, Current state of the art on tailoring the MXene composition, structure, and surface chemistry, *Curr. Opin. Solid State Mater. Sci.*, 2019, **23**(6), 100774.
9 F. Wan, X. Wang, C. Tang, C. Jiang, W. Wang, B. Li, Y. Zhang and X. J. A. Zhu, Metallic 1T-MoS_2 coupled with MXene towards ultra-high rate-capabilities for supercapacitors, *J. Mater. Chem. A*, 2022, **10**(22), 12258–12268.
10 L. Kashefi-Kheyrabadi, A. Koyappayil, T. Kim, Y.-P. Cheon and M.-H. Lee, A MoS_2@$Ti_3C_2T_x$ MXene hybrid-based electrochemical aptasensor (MEA) for sensitive and rapid detection of Thyroxine, *Bioelectrochemistry*, 2021, **137**, 107674.
11 W. Zheng, B. Sun, D. Li, S. M. Gali, H. Zhang, S. Fu, L. Di Virgilio, Z. Li, S. Yang and S. Zhou, Band transport by large Fröhlich polarons in MXenes, *Nat. Phys.*, 2022, **18**(5), 544–550.
12 M. Naguib, M. W. Barsoum and Y. Gogotsi, Ten years of progress in the synthesis and development of MXenes, *Adv. Mater.*, 2021, **33**(39), 2103393.
13 A. S. Zeraati, S. A. Mirkhani, P. Sun, M. Naguib, P. V. Braun and U. Sundararaj, Improved synthesis of $Ti_3C_2T_x$ MXenes resulting in exceptional electrical conductivity, high synthesis yield, and enhanced capacitance, *Nanoscale*, 2021, **13**(6), 3572–3580.
14 S. S. Sangu, N. M. Illias, C. C. Ong, S. C. B. Gopinath and M. S. M. Saheed, MXene-based aptasensor: characterization and high-performance voltammetry detection of deoxynivalenol, *BioNanoScience*, 2021, **11**, 314–323.
15 U. Amara, I. Hussain, M. Ahmad, K. Mahmood and K. Zhang, 2D MXene-based biosensing: a review, *Small*, 2023, **19**(2), 2205249.

Published on 03 2 2025. Downloaded on 2026/06/01 19:16:11.

16 A. Rhouati, M. Berkani, Y. Vasseghian and N. Golzadeh, MXene-based electrochemical sensors for detection of environmental pollutants: A comprehensive review, *Chemosphere*, 2022, **291**, 132921.
17 P. K. Kalambate, N. S. Gadhari, X. Li, Z. Rao, S. T. Navale, Y. Shen, V. R. Patil and Y. Huang, Recent advances in MXene–based electrochemical sensors and biosensors, *TrAC, Trends Anal. Chem.*, 2019, **120**, 115643.
18 X. Wu, P. Ma, Y. Sun, F. Du, D. Song and G. Xu, Application of MXene in electrochemical sensors: a review, *Electroanalysis*, 2021, **33**(8), 1827–1851.
19 S. Kumar, Y. Lei, N. H. Alshareef, M. Quevedo-Lopez and K. N. Salama, Biofunctionalized two-dimensional Ti_3C_2 MXenes for ultrasensitive detection of cancer biomarker, *Biosens. Bioelectron.*, 2018, **121**, 243–249.
20 X. Yang, M. Feng, J. Xia, F. Zhang and Z. Wang, An electrochemical biosensor based on AuNPs/Ti_3C_2 MXene three-dimensional nanocomposite for microRNA-155 detection by exonuclease III-aided cascade target recycling, *J. Electroanal. Chem.*, 2020, **878**, 114669.
21 P. A. Rasheed, R. P. Pandey, T. Gomez, K. A. Jabbar, K. Prenger, M. Naguib, B. Aïssa and K. A. Mahmoud, Nb-based MXenes for efficient electrochemical sensing of small biomolecules in the anodic potential, *Electrochem. Commun.*, 2020, **119**, 106811.
22 R. Chen, L. Kan, F. Duan, L. He, M. Wang, J. Cui, Z. Zhang and Z. Zhang, Surface plasmon resonance aptasensor based on niobium carbide MXene quantum dots for nucleocapsid of SARS-CoV-2 detection, *Microchim. Acta*, 2021, **188**(10), 316.
23 N. Arif, S. Gul, M. Sohail, S. Rizwan and M. Iqbal, Synthesis and characterization of layered Nb_2C MXene/ZnS nanocomposites for highly selective electrochemical sensing of dopamine, *Ceram. Int.*, 2021, **47**(2), 2388–2396.
24 W. Hong, B. C. Wyatt, S. K. Nemani and B. Anasori, Double transition-metal MXenes: Atomistic design of two-dimensional carbides and nitrides, *MRS Bull.*, 2020, **45**(10), 850–861.
25 B. Anasori, Y. Xie, M. Beidaghi, J. Lu, B. C. Hosler, L. Hultman, P. R. Kent, Y. Gogotsi and M. W. Barsoum, Two-dimensional, ordered, double transition metals carbides (MXenes), *ACS Nano*, 2015, **9**(10), 9507–9516.
26 J.-A. Yan and M. Chou, Oxidation functional groups on graphene: Structural and electronic properties, *Phys. Rev. B: Condens. Matter Mater. Phys.*, 2010, **82**(12), 125403.
27 A. C. Langedijk and L. J. Bont, Respiratory syncytial virus infection and novel interventions, *Nat. Rev. Microbiol.*, 2023, **21**(11), 734–749.
28 I. N. Mammas, S. B. Drysdale, B. Rath, M. Theodoridou, G. Papaioannou, A. Papatheodoropoulou, E. Koutsounaki, C. Koutsaftiki, E. Kozanidou and V. J. Achtsidis, Update on current views and advances on RSV infection, *Int. J. Mol. Med.*, 2020, **46**(2), 509–520.
29 B. S. Graham, Biological challenges and technological opportunities for respiratory syncytial virus vaccine development, *Immunol. Rev.*, 2011, **239**(1), 149–166.
30 Y. N. Löwensteyn, N. I. Mazur, H. Nair, J. E. Willemsen, G. van Thiel and L. Bont, Describing global pediatric RSV disease at intensive care units in GAVI-eligible countries using molecular point-of-care diagnostics: the RSV GOLD-III study protocol, *BMC Infect. Dis.*, 2021, **21**, 1–10.
31 C. Prendergast and J. Papenburg, Rapid antigen-based testing for respiratory syncytial virus: moving diagnostics from bench to bedside?, *Future Microbiol.*, 2013, **8**(4), 435–444.
32 A. Thakur, N. Chandran Bs, K. Davidson, A. Bedford, H. Fang, Y. Im, V. Kanduri, B. C. Wyatt, S. K. Nemani and V. Poliukhova, Step-by-step guide for synthesis and delamination of $Ti_3C_2T_x$ MXene, *Small Methods*, 2023, **7**(8), 2300030.
33 S. S. Shankar, R. M. Shereema and R. Rakhi, Electrochemical determination of adrenaline using MXene/graphite composite paste electrodes, *ACS Appl. Mater. Interfaces*, 2018, **10**(50), 43343–43351.
34 C.-C. Tsai and G. Wang, A glucose biosensor based on a 3D nanostructured gold electrode, *J. Electrochem. Soc.*, 2012, **160**(1), B1.
35 S. Srivastava, M. A. Ali, S. Umrao, U. K. Parashar, A. Srivastava, G. Sumana, B. Malhotra, S. S. Pandey and S. Hayase, Graphene oxide-based biosensor for food toxin detection, *Appl. Biochem. Biotechnol.*, 2014, **174**, 960–970.
36 Y. Li, W. Y. Lieu, T. Ghosh, L. Fu, X. Feng, A. J. Y. Wong, A. Thakur, B. C. Wyatt, B. Anasori and Q. Zhang, Double-Transition-Metal MXene Films Promoting Deeply Rechargeable Magnesium Metal Batteries, *Small Methods*, 2023, **7**(8), 2201598.
37 S. Shahriari, M. Sastry, S. Panjikar and R. Singh Raman, Graphene and Graphene Oxide as a Support for Biomolecules in the Development of Biosensors, *Nanotechnol., Sci. Appl.*, 2021, 197–220.

 This journal is © The Royal Society of Chemistry 2025